Unraveling the implications of multiple histidine residues in the potent antimicrobial peptide Gaduscidin-1

Jasmin Portelinha,[a] Kara Heilemann,[a] Jing Jin,[b] Alfredo M. Angeles-Boza[*,a,c]

a Department of Chemistry, University of Connecticut, 55 N. Eagleville Road, Storrs, CT 06269

b Magnetic Resonance Center, Boston College, 2609 Beacon Street, Chestnut Hill, MA 02467

c Institute of Material Science, University of Connecticut, 97 N. Eagleville Road, Storrs, CT 06269

*Corresponding author: alfredo.angeles-boza@uconn.edu, Phone: 860-486-6718.

ABSTRACT: The development of antimicrobial peptides (AMPs) as potential therapeutics requires resolving the foundational principles behind their structure-activity relationships. The role of histidine residues within AMPs remains a mystery despite the fact that several potent peptides containing this amino acid are being considered for further clinical development. Gaduscidin-1 (Gad-1) is a potent AMP from Atlantic cod fish that has a total of five His residues. Herein, the role of His residues and metal-potentiated activity of Gad-1 was studied. The five His residues contribute to the broad-spectrum activity of Gad-1. We demonstrated that Gad-1 can coordinate two Cu^{2+} ions, one at the N-terminus and one at the C-terminus, where the C-terminal binding site is a novel Cu^{2+} binding motif. High affinity Cu^{2+} binding at both sites was observed using mass spectrometry and isothermal titration calorimetry. Electron paramagnetic resonance was used to determine the coordination environment of the Cu^{2+} ions. Cu^{2+} binding was shown to be responsible for an increase in antimicrobial activity and a new mode of action. Along with the traditional AMP mode of action of pore formation, Gad-1 in the presence of Cu^{2+} (per)oxidizes lipids. Importantly, His3, His11, His17, and His21 were found to be important to lipid (per)oxidation. This insight will help further understand the inclusion and role of His residues in AMPs, the role of the novel C-terminal binding site, and can contribute to the field of designing potent AMPs that bind metal ions to potentiate activity.

1. INTRODUCTION

Antimicrobial peptides (AMPs) are ubiquitous in nature as they evolved through adaptive radiation and are currently found in prokaryotes and eukaryotes. Identifying key structural and physicochemical patterns such as prevalence of α-helicity, cationicity, and amphipathicity, via quantitative structure activity relationship studies or computationally based approaches[1], such as machine-learning, has shed light on the immunological role of AMPs and provided a pathway for the translation of these ancient immune molecules into preclinical development. Among AMPs, the most common residues are Lys, Gly, Leu, Ala, and Val, whereas the least common amino acids are Pro, Cys, Tyr, and His. In the 3217 peptides in the Antimicrobial Peptide Database, His appears in only 2.2% of them.[2] Moreover, a recent bioinformatic and pattern recognition study found His residues are underrepresented in eukaryotes as less than 2% contain them.[3] Despite this low representation, there are important families of peptides, such as the piscidins, histatins and clavanins (Figure 1), to name but a few in which His represents anywhere from 13-29% of their residues.[4–6] Piscidins are the most common family of AMPs present in a wide range of teleost fish taxa with broad-spectrum activity, and unlike most AMPs, are active at high ionic strengths and low pH environments.[5,7] If we are to find a unifying model of molecular characteristics that describe the antimicrobial properties of peptides and use it to develop AMP therapeutics, specifically those that can take advantage of metal ions utilized by our immune system,[8,9] we need to understand the role of His residues in AMPs.

The N-terminus of piscidin peptides are highly hydrophobic and conserved, with Phe and Ile residues, which can facilitate entry into the lipid bilayer, but are less uniform at the C-terminus (Figure 1). The N-terminus is almost always comprised of an amino terminal copper and nickel (ATCUN) binding motif that has been shown to contribute to the multi-hit mechanism utilized by piscidin peptides to kill pathogens. The multi-hit nature of piscidin peptides is comprised of a membrane-active component through the formation of ion channels and lipid (per)oxidation,

as well as an intracellular component that involves DNA binding and damage.[7,10–14] The broad-spectrum activity and DNA binding is enhanced by inclusion of His and Arg residues and a $G(X)_4G$ motif in the center of the peptides that induces flexibility and allows easier binding to DNA.[15,16] The metal binding nature of piscidins is relevant *in vivo* because piscidins are found in phagocytic cells.[5,7] Metal ions such as Cu^{2+} and Zn^{2+} have been observed at high micromolar concentrations in the phagocytic milieu of several species as a response to certain types of infections.[17–20] Piscidin-Cu interactions have been studied previously and revealed that piscidin 1 and piscidin 3 can induce an SOS response in *Escherichia coli* and piscidin 2 has been found to have partial synergism with Cu^{2+} against fungi.[10,21] Atlantic cod ubiquitously produces the piscidins Gaduscidin-1 (Gad-1, FIHHIIGWISHGVRAIHRAIH-NH_2), Gaduscidin-2 (Gad-2, FLHHIVGLIHHGLSLFGDR-NH_2), and pis-2β, a splice variant.[22] Gad-1 and Gad-2 are both active against bacteria, however, Gad-1 is more active at physiological and low pH than Gad-2.[22–24] In contrast, Gad-2 is more active against the parasite *Tetrahymena pyriformis* than Gad-1.[22,23] These examples showcase the impact that small modifications on the AMPs scaffold can have on their antimicrobial activity. Gad-1 contains five His residues, one of them in the ATCUN motif FIH, whereas the others are found in positions 4, 11, 17, and 21. As shown in Figure 1, the $H_{17}XXXH_{21}$ motif is uncommon among piscidins, making Gad-1 a good candidate to study the implications of multiple metal binding sites on AMPs.

Herein, Gad-1 was studied to elucidate the role of the His residues vis-à-vis metal binding and mechanism of action. The antimicrobial activity of Gad-1 and the influence of metal binding at both sites, including the unique HXXXH motif, on the antimicrobial activity was investigated. The ability for Cu^{2+} to bind to Gad-1 at the ATCUN and HXXXH site was probed using electrospray ionization mass spectrometry (ESI-MS) and isothermal titration calorimetry (ITC). Moreover, coordination geometry was studied using electron paramagnetic resonance (EPR) to investigate the HXXXH binding site coordination and it revealed that the coordination

is either through four nitrogen bonds or through three nitrogen bonds and one oxygen bond. The peptide can bore holes in the membrane, however, when Cu^{2+} is available, Gad-1 can additionally peroxidize lipid membranes to enhance activity. This work furthers our understanding of the role of His residues in AMPs and how they can potentiate antimicrobial activity. It also broadens our knowledge on the coordination chemistry of the HXXXH motif and establishes that HXXXH bound to Cu^{2+}, a departure from the mechanism elucidated for HXXXH with Zn^{2+} in the marine AMP, Clavanin A.[25,26] To our knowledge this is the first study to examine biophysical and mechanistic advantages for AMPs with multiple metal binding sites.

2. EXPERIMENTAL METHODS

2.1 Materials

*Any water used was obtained from a Barnstead NANOpure Diamond filtration system with a 0.2 micron pore size filter. All chemicals are from Sigma Aldrich unless otherwise specified. All media that was used had a pH of 7.0 +/- 0.1 unless otherwise specified.

2.2 Peptide synthesis and purification

Peptide synthesis and purification methods have been previously published.[27] Gad-1, H3A. H4A, H11A, H17A, and H21A was synthesized in our lab, however, additional Gad-1, H3A, and H17A peptide was purchased from Atlantic Peptides. The peptides were all purified to >94% before using.

2.3 MIC and MBC measurements

All minimum inhibitory concentration (MIC) assays utilized sterile 96-well polypropylene round bottom plates (Grenier). A 105 μL aliquot of the peptide, at 256 μM, was prepared in Mueller Hinton Broth (MHB) media. In column one of the plate, 100 μL of the peptide solution was plated. A 2-fold serial dilution was done until column 10. A sterility control contained 100

μL of MHB and a positive control consisted of 50 μL MHB and a 50 μL aliquot of bacteria. A 10 mL MHB culture was inoculated with two to five colonies of *E. coli* MG1655 and incubated at 37˚C for four hours (midlog phase OD600~0.4). A 50 μL aliquot of the inoculum was added to all wells except the sterility control, making the final concentration of cells $5X10^5$. Plates were examined after 18-20 hours. The MIC was determined based on visual turbidity, with the MIC being the lowest concentration where growth did not occur. The minimum bactericidal concentration (MBC) was subsequently determined by plating 10 μL of inoculum to a Luria Broth (LB) plate at MIC concentration and two times the MIC concentration. The plate was incubated for 18-20 hours at 37˚C and colony growth was observed. MIC and MBC values are reported as the mode and the data is representative of at least three trials. The MIC in the presence of triethylenetetramine (TETA) was run with 400 μM TETA that was added to the media to ensure that there was no labile Cu^{2+} ions. When using *Vibrio harveyi* and *Aeromonas hydrophila* LB with 2% and 1% NaCl, respectively, was used, as these are optimal growth conditions for these pathogens. The MIC and MBC plates were grown for three days at room temperature.

2.4 Time kill kinetics measurements

Two to five *E. coli* MG1655 colonies were inoculated in a 10 mL MHB culture and incubated at 37˚C for four hours. The bacteria were diluted in MHB media to $1X10^6$ cells. Peptide solutions at a concentration of 8 μM were prepared in MHB media in a volume of 350 μL. The peptide solutions were added to 350 μL of diluted *E. coli* in a 5 mL polypropylene tube. The positive control consisted of 350 μL of MHB inoculated with 350 μL of *E. coli*. The samples were incubated at 37˚C in a shaking incubator. At each time point the samples were diluted appropriately (up to 10,000 fold) into MHB and 100 μL was plated and spread on LB plates immediately after adding the bacteria at zero-hour and then at one-hour, two-hour, and four-

hour time points. Plates were incubated for 18-20 hours at 37˚C and colonies were counted to quantify the inhibition of growth. The data presented is representative of three trials.

2.5 ESI-MS experiments

A 10 mM Cu^{2+} stock was prepared with $CuSO_4$ in H_2O. Peptide (20 µL, 50 µM) was mixed with Cu^{2+} in H_2O using a ratio of 1:5 peptide:Cu^{2+} and incubated for 30-60 minutes before injection. The samples were run on a 4000-Q TRAP LC/MS/MS system by Applied Biosystems.

2.6 ITC experiments

Peptides (300 µM) were diluted with either 2-(N-morpholino)ethanesulfonic acid (MES) buffer at pH 5.5 or 3- (N-morpholino) propanesulfonic acid (MOPS) buffer at pH 7.0 and degassed for 20 minutes. The peptides were titrated with anywhere from 3000 to 10,000 µM Cu^{2+} at 25˚C over 20 injections, using a Nano-ITC from TA Instruments. The stir rate was 300 rpm. Cu^{2+} into buffer was used as a blank and was subtracted from all measurements. Two trials were averaged and analyzed on NanoAnalyze software (v3.11.0) from TA Instruments. The data was fit to a multiple site fitting model (lowest residual model was used for Gad-1) or an independent binding model. MOPS buffer-metal interactions were corrected for K_d and ΔH using Quinn *et al.*[28]

2.7 EPR experiments

Sample concentrations ranged from 200 µM to 1 mM peptide, depending on the solubility in MOPS buffer at pH 7.0. A ratio of 1:0.9 peptide:Cu^{2+} was used and the sample was prepared in 10% glycerol in either MOPS buffer at pH 7.0 or in MOPS buffer and trifluoroethanol (TFE) (50:50). The samples were transferred to quartz EPR tubes and frozen in liquid nitrogen. Samples were run at 50 K using liquid helium on a Bruker cw-ESR EMX spectrometer with X-

Band bridge. X-band data was collected with a microwave frequency of 9.32 GHz. The microwave power was 0.06325 mW and the sweep width was 1200 G. The spectra were collected and averaged using 4 to 12 scans. Titration samples were run and aliquots of Cu^{2+} stock in MOPS were added and the sample was run again. MATLAB and Xenon Nano Biospin Bruker software was used to produce spectra and find g values. The simulation was carried by Aniso-SpinFit program. It is a built-in program in Bruker's Xenon software, which is designed for the simulation of the solid or frozen system.

2.8 Circular dichroism (CD) measurements

The peptides were diluted to 50 μM in 300 μL of H_2O or a 50:50 H_2O:TFE mixture. They were run on the Applied Photophysics π*-18C instrument in a 0.1-cm quartz cuvette at room temperature. Each sample was run with two replicates at 1.0 nm intervals from 250-190 nm. The bandwidth was 3 nm. When metal ions were added to the peptide samples, they were incubated for 45 to 60 minutes before analysis. The data was input into Beta Structure Selection (BeStSel) algorithm (http://bestsel.elte.hu/index.php) to determine the secondary structure.[29]

2.9 β-galactosidase leakage assay

E. coli, transformed with the plasmid pUC19, was grown to an OD600 of 0.4 to 0.6. The cells were induced by 1 mM isopropyl β-D-1thiogalactopyranoside for one hour and washed with 5 mL of phosphate buffered saline (PBS) with a pH of 7.4, three times for ten minutes. The cells were resuspended to a culture volume of 10 mL of pH 7.4 PBS. A 75 μL aliquot of bacteria was incubated with 75 μL of peptide, diluted in pH 7.4 PBS, at a final concentration of 2 μM. The samples were incubated at 37˚C for one hour. The tubes were centrifuged for ten minutes at 4˚C. A 100 μL aliquot of supernatant was added to 50 μL of 8 mg/mL o-nitrophenyl-β-D-galactopyranoside (ONPG, freshly prepared) in PBS. The 150 μL was plated in a 96-well plate and read at 405 nm every five minutes for one hour. The data is represented as a percentage where 0.1% Triton X-100 is 100%. The negative control was PBS mixed with ONPG and this

was subtracted from all values before calculating the percentages. Data from the one-hour time point was used and a total of three to four trials were done to confirm the activity.

2.10 Lipid (per)oxidation assay

MWF1, fabR::kan recD::Tn10, an *E. coli* strain with a high number of unsaturations in the bilayer, was grown for four hours and washed three times with 20 mM 2-[4-(2-hydroxyethyl)piperazin-1-yl]ethanesulfonic acid (HEPES) and 100 mM NaCl buffer at pH 7.4. Cells were resuspended in 10 mL of buffer and diluted to $2X10^7$ cells. Peptide solutions were prepared in buffer at two times the final concentration (4 μM). An aliquot of 50 μL of diluted bacteria and 50 μL of peptide solution were added and incubated for two hours at 37˚C. Once the treatment concluded, 100 μL of trichloroacetic acid (1% w/v) was added to each sample, followed by 800 μL of colorimetric reagent (106 mg thiobarbituric acid, 10 mL of 0.7 M NaOH, and 10 mL of 20% acetic acid). Samples were vortexed and added to a dry heat block at 97˚C for 60 minutes. Samples were put in a -20˚C freezer for 10-20 minutes to cool to room temperature. Samples were centrifuged for ten minutes at 4˚C and a 200 μL aliquot was added to a 96-well black plate in duplicate. The fluorescence was recorded at 530 nm excitation and 550 nm emission and relative fluorescence intensity is reported using an Agilent CARY Eclipse fluorimeter. Standards (0-5 μM) were run using 1,1,3,3-tetramethoxypropane, diluted in buffer. Data is representative of four to five trials and the standard error is reported. A student t-test was used to determine statistical significance.

3. RESULTS AND DISCUSSION

3.1 Antimicrobial assays suggest that four His residues are essential to the activity of Gad-1

Gad-1 has previously been tested against Gram-negative and -positive pathogens, in addition to a parasite and showed <10 μM activity with almost all of the tested strains.[22] Here, Gad-1 was tested against the fish and human Gram-negative pathogens *V. harveyi*, *A. hydrophila*, and *E. coli*. The role of the His residues on the activity was probed through His to Ala mutant peptides. *V. harveyi* and *A. hydrophila* were tested to learn more about the efficacy of Gad-1 in the natural system, as these bacteria often infect cod fish. Gad-1 had low micromolar activity against both fish pathogens (Table 1) and was bactericidal at MIC concentrations based on the MBC, while the mutants lacking His residues had varied activity. In *V. harveyi*, H3A, H4A, and H11A mutants had lower activity when compared to Gad-1; however, H3A, H11A, and H17A were observed to be less active against *A. hydrophila*. Against *E. coli*, His3, His11, and His17 were the most important residues for antimicrobial activity as their mutations to Ala resulted in a decreased activity.

We hypothesize that H3A and H17A mutants likely have lesser activity due to the possibility of His3 and His17 being engaged in Cu^{2+} binding.[10,30] We tested this hypothesis by determining the MIC in the presence of TETA, an extracellular chelator with high affinity for Cu^{2+} used to treat acute copper intoxication.[31] Atomic absorption spectroscopy has shown that MHB contains ~80 μM Cu^{2+},[32] an amount that is sufficient to metallate Gad-1. The addition of TETA to the susceptibility assay reports on the requirement for Cu^{2+} ions by the peptide.[32] In the presence of TETA, all of the peptides had an MIC identical to the H3A mutant suggesting that Cu^{2+} binding elicits a stronger bactericidal response and activates an additional mode of action in Gad-1.

Since peptides with an HXXXH motif have been reported to enhance their activity in the presence of Zn^{2+} ions,[25,26,33,34] the susceptibility of *E. coli* towards Gad-1 was tested in MHB supplemented with Zn^{2+} ions. Gad-1 does not have potentiated antimicrobial activity in the presence of Zn^{2+} ions, as there was no change in the MIC values, even in the presence of ten

equivalents of Zn^{2+} (Table S1). This observation led to the conclusion that Zn^{2+} may not be relevant to the activity of Gad-1, therefore, we focused on Cu^{2+} interactions for the rest the experiments. The metal binding investigated here, seems to have more of an influence on the activity against *A. hydrophila* due to the loss of antimicrobial activity in the absence of residues His3 and His17, which are likely associated with metal binding sites. This phenomenon has also been observed in Drosophila, where certain AMPs can be more active against specific pathogens.[35,36] Similar to AMPs found in *Drosophila*,[35,36] Gad-1 may have also evolved to be more active against this pathogen because it commonly infects Atlantic cod fish. Overall, Gad-1 has antimicrobial activity against a variety of Gram-negative bacteria that is potentiated in the presence of Cu^{2+}.

In addition to using MIC measurements, time kill kinetics (TKK) data using *E. coli* was utilized to determine which residues were important to the bactericidal activity of Gad-1. The peptides were tested at 4 μM, which was chosen to avoid the concentration of Gad-1 being much larger than MIC concentrations. The results show that mutating any of the His residues in Gad-1 resulted in a decreased bactericidal activity, including complete abolishment for the H3A, H17A, and H21A (Figure 2). Interestingly, the H4A mutant had similar activity early on but it started deviating after 4 hours.

3.2 Cu^{2+} can bind to both the ATCUN and HXXXH motif

To examine the ability of Gad-1 to bind to metal ions and elucidate the role of each His residue in metal binding, ESI-MS was used. Addition of five equivalents of Cu^{2+} ions resulted in the formation of singly and doubly metallated species hinting at the possibility of an additional metal site besides the ATCUN motif (Figure 3A). To determine what residues were important for the binding of the second Cu^{2+} ion, we synthesized the H3A-H11A and H3A-H17A double mutants. When using the H3A-H17A double mutant there was no holo-species identified, whereas the H3A-H11A double mutant formed a 1:1 complex (Figure 3B). This result

suggests that His17 is required for Cu^{2+} binding on the second binding site, most likely the $H_{17}XXXH_{21}$ sequence (Figure 3C).

3.3 EPR evidence indicates that the Cu^{2+} is binding in a square planar coordination at the ATCUN and HXXXH sites

To gather more information about the environment of the Cu^{2+} binding sites, we used X-band EPR in Cu^{2+} coordination complexes of Gad-1 and its mutants. In Figure 4, the spectra show the X-band EPR data collected at 50 K for Gad-1, the H3A mutant, and the H17A-H21A double mutant in MOPS buffer at pH 7.0. The addition of 0.9 eq. of Cu^{2+} to Gad-1 and the double mutant resulted in species that displayed rhombic spectra, whereas H3A showed an axial spectrum under the same conditions, indicating that the ATCUN motif gives rise to the rhombic spectrum, while the HXXXH binding site is axial. All of the samples showed some residual unbound Cu^{2+}, which is exemplified by the extra aqua-Cu peak at ~2600 G[37] that may have resulted from inadequate binding or peptide solubility issues at high concentrations. The species that were observed for both binding sites are type II Cu complexes that display square planar coordination with $A_{\parallel}$ values of 120-200 G, which is the preferred coordination for Cu^{2+} (Table 2).[38] Another metric that was used to confirm coordination was $g_{\parallel}/A_{\parallel}$ values, where 130-150 cm indicates slightly distorted square planar.[37] The $g_{\parallel}/A_{\parallel}$ values for all three peptides tested confirms a slightly distorted square planar coordination for both binding sites EPR has been used previously to characterize the ATCUN binding, which shows peaks at ~2800, 3000, 3200, 3250, and 3400 G.[8,39–41] The average $g_{\parallel}$ value for the ATCUN motif is 2.19, $A_{\parallel}$ of 0.020 cm^{-1}, and $g_{\perp}$ is 2.05.[42] In Figure 4A, the H17A-H21A spectrum displays a distorted square planar coordination that is expected for the ATCUN motif, although peaks are slightly left shifted.[30] The H17A-H21A double mutant had a $g_{\parallel}$ and $g_{\perp}$ value that is slightly higher than traditional ATCUN motifs, while the $A_{\parallel}$ value was slightly lower expected. These slight deviations from average may be due to weak coordination to the nitrogen from His4 because higher

$g_{\parallel}$ values are consistent with binding to an increased number of nitrogens.[38] Five coordinate species of Cu^{2+} are not uncommon, although they have not been reported for ATCUN-Cu^{2+} complexes.[43,44] A study on the ATCUN-containing AMP piscidin 3 (FIHHIFRGIVHAGRSIGRFLTG-NH_2) bound to Ni^{2+} recently showed His4 is in close proximity to the metal center and could be involved in binding.[45] An ATCUN site binding to Cu^{2+} can easily accommodate a fifth ligand as demonstrated by the Cu(II) complex of neuromedin C (GNHWAVGHLMNH_2) which contains a cation-π interaction with the indole ring of the Trp residue.[46]

In regards to the HXXXH motif, the H3A spectrum revealed an axial orientation and likely square planar coordination due to the values aligning with known square planar complexes, where $g_{\perp}$ is greater than 2.0, $g_{\parallel}$ is greater than 2.1 and $A_{\parallel}$ is between 160 to 210 10^{-4} cm^{-1}.[8,37] When H3A was titrated with Cu^{2+}, there appeared to be super hyperfine splitting (shf) from 3200-3300 G (Figure S2). Seven lines in the shf region is indicative of coordination to three nitrogen atoms, while nine lines is indicative of coordination to four nitrogen atoms.[47,48] It was inconclusive how many lines and further experiments could not clarify the shf, however, there are at least seven lines and therefore at least three nitrogen atoms coordinated to the Cu^{2+} likely two of which are from the imidazole rings of His17 and His21.[38] To clarify what ligands are coordinated to Cu^{2+} at the HXXXH site, a Peisach-Blumberg plot was used and the $g_{\parallel}$ and $A_{\parallel}$ values for the H3A spectrum corresponds to either 2N2O, 3N1O, or 4N atoms due to overlap in the chart.[49] It may be possible that the proximity of Arg18 and the amidated C-terminus could contribute other nitrogen ligands but the data is inconclusive at this time.[50–52] We are currently further investigating the coordination using 2D NMR techniques. Using the collective data, the coordination at the HXXXH site is likely to two imidazole rings and either two other nitrogens or one nitrogen and a water molecule.

When Gad-1 was titrated with Cu^{2+} (Figure 4B), there were clear changes in the spectra as more Cu^{2+} was added, which reinforced the idea that there are two different types of Cu^{2+} binding. There is an appearance of a new peak at 3250 G that likely corresponds to the HXXXH site and can be linked to the second site due to g values that resemble the H3A sample. There is a growing peak at 3200 G that resembles the signal obtained when 0.9 equivalents of Cu^{2+} were added to Gad-1 in 50% TFE, a solvent combination that promotes helicity (*vide infra*) (Figure 4C (boxed)) and it likely corresponds to the HXXXH site. Simulations were utilized to determine how many species were present when H3A and the H17A-H21A double mutant were exposed to Cu^{2+} (Figure 5). It was confirmed that the H3A spectrum with 0.9 equivalents of Cu^{2+} only consisted of one species in MOPS buffer and was different from the spectrum of the H17A-H21A double mutant. This data supports the conclusion that there are two different binding modes for Cu^{2+} in Gad-1, one being the ATCUN motif and the other being the HXXXH motif. Interestingly, the H17A-H21A double mutant had one major species and one minor species, based on the simulation data. The HXXXH motif could be binding Cu^{2+} through the imidazole of His17, His21, with either one water molecule and an additional nitrogen or two nitrogens, possibly from $Arg18^{50–52}$ and the amidated C-terminus in a square planar fashion. His4 is likely able to weakly coordinate to Cu^{2+} in the ATCUN motif to further stabilize Cu^{2+} binding.

3.4 Gad-1 has two high affinity Cu^{2+} binding sites at low and physiological pH

ITC was utilized to determine the binding affinity of Cu^{2+} at both binding sites, along with thermodynamic and stoichiometric constants. It was expected that the ATCUN motif would have high affinity binding for Cu^{2+}.[53–55] Titrations were done in MOPS buffer (pH 7.0) and MES buffer (pH 5.5) using 300 μM peptide and varied concentrations of Cu^{2+}. Gad-1 was used to determine the binding constant for both sites by fitting to a multiple site model (Figure S3). Low and physiological pH were used to investigate any differences in binding affinity and to

determine whether the binding is relevant within the range of pH evaluated. It is well known that buffers interact with metal ions to some extent, therefore, a correction for the presence of MOPS buffer at pH 7.0 was used, however, there was no available correction for MES buffer or any other Good's buffer at pH 5.5, therefore, buffer correction could only be done for the pH 7.0 titration.[28] The stoichiometries, n (Table 3), are close to 1, as expected for the complexation of one Cu^{2+} ion to each binding site. Deviations from n = 1 are observed and are either due to slight errors in solution concentrations or an artifact of fitting the data to a two-site model, which has been observed before by Zhang *et al*.[56,57] By manipulating the concentrations in the software, the n value can be forced to be 1, but this may result in a different, poorer fit to the data and was not done here.[56,57] At pH 7.0, the ATCUN binding site exhibited high affinity for Cu^{2+} ions (K_d = 5.46 × 10^{-13} M), consistent with other ATCUN sites such as those in histatin 5 and human serum albumin.[58,59] This value is also similar to the AMP piscidin 1, which has a reported K_d of 3.29 × 10^{-13} M, and shares a His residue in position 4 that may contribute to the stability of binding by forming a hydrophobic fence.[10] The second binding site, which we assign to the HXXXH sequence, has a weaker binding towards Cu^{2+} (5.92 × 10^{-10} M). At pH 5.5, the uncorrected K_d values were lower for the two binding sites as expected due to the competition for protonation of the atoms coordinating to the metal ions. Similarly, to the results at pH 7.0, the ATCUN binding was stronger than the HXXXH binding by three orders of magnitude (Table 3). The binding constant at the second site was also measured using an H3A mutant. The values at pH 7.0 and pH 5.5 coincided well with the measured value in the wild type, validating the multiple binding site model (Table 4). The H4A mutant yielded similar binding constants and thermodynamic parameters at both pH values compared to the wild type. Interestingly, a double H17A-H21A mutant was tested and the data collected at pH 7.0 fit to a multiple binding site model, while at pH 5.5 the binding was fit to an independent binding site model. The values at pH 5.5 coincided with the thermodynamic values that were observed for

the ATCUN site with the wild type and H4A peptides (Table 4). There may not be binding to the second site here due to protonation of the His residues that may initiate metal binding. In terms of the pH 7.0 conditions, the values for the ATCUN site are also similar to the wild type conditions, however the K_d value for the second site was significantly weaker by two orders of magnitude (Table 4). We expected that based on the other evidence that the second binding event would not have occurred when His17 and His21 were removed, but it is clear that these residues are required for stronger binding interactions. We are currently investigating this discrepancy with 2D NMR techniques to enhance our understanding of the binding interactions at the C-terminal site.

Coordination to Zn^{2+} at one site on Gad-1, likely the HXXXH site, was also shown using MS (Figure S1). The K_d for the second binding site was also assessed using Zn^{2+} at both pH conditions, however, no correction factors are available for these buffer conditions with Zn^{2+}, therefore, it is difficult to compare the values to Cu^{2+} binding (Table S2). Although the comparison is difficult to make here, it is likely that Cu^{2+} will have stronger affinity than Zn^{2+} for the binding sites according to the Irving-Williams series.[60] The binding at pH 7.0 yielded a K_d of 2.831×10^{-4} and the thermodynamic parameters were consistent with metal binding (-ΔH, +ΔS). These values are consistent with a Zincon binding titration that showed that the K_d must be weaker than 12.6 μM because the peptide could not outcompete Zincon (Figure S1). The K_d at pH 5.5 was at the lowest limit of detection for the ITC ($>1 \times 10^{-3}$ M) indicating that the binding is likely too weak to measure with this method. *In vivo* these K_d values would likely be lesser, possibly by several orders of magnitude due to higher salt concentrations and other components of the cellular milieu. However, based on these binding affinities, it is likely that the ATCUN motif plays an important role throughout all the pH range found in acidophilic granulocytes, whereas the HXXXH binding site plays a larger antimicrobial role at physiological pH rather than at lower pH.[61,62] *In vivo*, both sites in the peptide can utilize metal-mediated activity and

will be effective at killing extracellularly in a phagocytic burst.[61,62] AMPs with multiple binding sites may be more adaptable due to their ability to strongly bind metal under varied pH conditions and in different cellular spaces when compared to other AMPs that may not be able to bind metal.

3.5 Holo-Gad-1 does not have increased helical stability

It has been observed that the antimicrobial activity of several AMPs is affected by the change in helicity, where the relationship is typically directly proportional. CD was employed to determine the secondary structure of the peptides. The peptides showed a high percentage of α-helicity in 50:50 TFE:H_2O and were disordered in H_2O (Figure 6). This is consistent with existing data on Gad-1 that reported an α-helical structure in POPG, POPC, and SDS micelles based on CD and NMR experiments.[23] H4A and H21A had the lowest degree of helicity followed by Gad-1, while H3A, H11A, and H17A were the most helical (Table 5). Interestingly, the helicity of H4A and H21A decreased but the β-sheet character increased significantly compared to Gad-1 and the other mutant peptides. Based on the helical wheel diagram (Figure S4), some of these changes in helicity are unexpected. Substitution of His21 should not result in a large change compared to Gad-1 because it is at the end of the sequence. Additionally, the substitution of His3, His4, and His17 were expected to yield higher helicity due to these residues being surrounded by hydrophobic residues such as Phe1, Trp8, Val13, and Ile20 but His4 was less helical than Gad-1. His11 is part of the $G(X)_4G$ helix breaking motif yet it yielded a higher percent helicity. This may be due to the propensity for Ala residues to induce helicity when not placed in hydrophilic regions of the peptide.[63] The secondary structure of Gad-1 in the presence of metal ions did not change substantially and cannot be responsible for the increased activity of the holo-Gad-1 species. Our group has previously shown that there is not a large change in CD spectrum or helicity of a peptide when they are metal bound.[26] Figure 6C

shows the same trend with Gad-1, where in the presence of excess Cu^{2+} there was no change in helicity (Table 5). Overall, secondary structure of Gad-1 is consistent with previously collected data, indicating it forms an α-helix in the presence of TFE and that there is no clear stabilization of secondary structure upon metal binding that can account for increased antimicrobial activity.

3.6 Holo-Gad-1 targets membranes, forms pores, and peroxidates lipids via ROS formation

Since we did not observe a strong correlation between helicity and antimicrobial activity, we decided to look at other possible factors affecting the activity of Gad-1. A number of AMPs have been shown to permeabilize the bacterial membrane.[16,64,65] The ability to form pores in the membrane is modulated in part by amphipathicity of the peptide, therefore, Gad-1 should have at least some membranolytic activity due to the near perfect amphipathic nature of Gad-1 (Figure S4). The peptides were tested for membrane activity against *E. coli* using a β-galactosidase leakage assay. All mutant peptides had similar membranolytic activity compared to Gad-1, which is consistent with a one amino acid substitution that should not drastically alter amphipathicity (Figure 7A). The peptides were all ~50% lytic at 2 μM compared to Triton X-100, even considering that the mutants are at sub-MIC concentrations (Table 5). This suggests that at least part of the lethality of Gad-1 is modulated by pore formation.

The possibility of a multi-hit nature of Gad-1 led to testing of another probable mechanism of action, namely lipid (per)oxidation, likely to occur when lipids are exposed to Cu-bound ATCUN-AMPs.[66] Lipid (per)oxidation can occurred by Fenton-like chemistry that produces reactive oxygen species (ROS).[67] For example, the tick ATCUN-AMP ixosin, was previously shown to have greater lipid (per)oxidation abilities compared to its H3A mutant, which cannot bind to Cu^{2+}.[66] Other non-metalloAMPs and antibiotics can also use ROS to kill pathogens and

contribute to their bactericidal activity.[68,69] Using a standard thiobarbituric acid reactive substances (TBARS) assay with an *E. coli* mutant containing an increased concentration of unsaturated lipids, Gad-1 and its mutants were analyzed for production of lipid (per)oxidation. Gad-1 and the mutants were all seen to peroxidize lipids to some extent (Figure 7), however, when one equivalent of Cu^{2+} was preincubated with peptide, the amount of lipid (per)oxidation increased 1.4, 2, and 1.7 times for Gad-1, H4A, and H17A, respectively. Under the assay conditions, Cu^{2+} alone did not elicit any notable (per)oxidation when tested at 8 and 16 μM, indicating that if the Cu^{2+} was not able to bind the peptide it would not have significantly changed the amount of basal lipid (per)oxidation. Due to the nature of the assay, it is also plausible that cellular death can lead to oxidative process that do not depend directly on the ATCUN-Cu^{2+} complex, as it has been seen for several antibiotics.[68,70,71] The addition of the Cu^{2+} chelator TETA inhibited the amount of lipid (per)oxidation, which strengthens the argument that this lipid (per)oxidation originates from the presence of Cu^{2+} and the peptide. These results confirm that His3 is important to the ROS formation propagated by holo-Gad-1, much like other ATCUN-peptides. The H11A mutant did not produce a significant amount of lipid (per)oxidation, a phenomenon that we cannot explain at the moment and should be investigated further. It may be possible that the increased helicity of the H11A mutant could be involved, however, there is no direct evidence to support this. Incubation of cells with the H17A and H21A mutants resulted in decreased lipid (per)oxidation as compared to the wild type when the additional metal ion was present, suggesting that Cu^{2+} bound to this second binding site can also produce ROS to contribute to increased oxidative damage. This is not surprising as a number of Cu^{2+} complexes containing ligands with N and O donor atoms produce ROS.[72–74] Molecular dynamics simulations done by Khatami *et al*. showed that the 3rd and 17th residues in Gad-1 interact with lipids in the bilayer, thus, it is possible that upon Cu^{2+} binding, the lipids are directly exposed to ROS produced by the ATCUN and HXXXH sites.[75]

4. CONCLUSIONS

Piscidins are a diverse family of AMPs that have potent activity and an unusual presence of His residues. Gad-1 is a member of this family that contains five His residues and is potent against human and fish Gram-negative bacteria. Our studies hint at a multi-hit mechanism for Gad-1 and reveal a potential role for the His residues in the sequence. This is important because a multi-hit mode of action increases the lethality of the AMPs and may confer an advantage for the host as pathogens find it more difficult to develop resistance. It is likely that the multi-hit mechanism of Gad-1 is not limited to pore formation and lipid (per)oxidation since at least one piscidin peptide, piscidin 3, has been found to enter cells at sub-MIC concentrations and damage bacterial DNA. We are currently investigating other intracellular and metal-mediated modes of action of Gad-1. We conclude that a key role for the presence of all these His residues is to take advantage of the pool of Cu^{2+} ions found in phagosomes and other sites of hosts battling pathogens. Based on ESI-MS and ITC data, Gad-1 was shown to be able to bind Cu^{2+} with high affinity at the ATCUN and HXXXH sites. The Cu^{2+} environment in both coordination sites was investigated using EPR. Our studies revealed that the HXXXH site binds to the metal ion along with either two other nitrogen atoms or one other nitrogen and one water molecule in a square planar geometry. Additional insight from EPR experiments revealed that His4 is also coordinating Cu^{2+} at the ATCUN binding site to further stabilize metal binding.

Overall, this work adds to the understanding of AMPs, specifically the role played by His residues. It is clear that to obtain a holistic theory of AMPs, we need to define the foundational principles that characterize His-rich AMPs. This knowledge can later be applied to the design of AMPs that can combat antibiotic resistant pathogens.

Supporting Information

Supporting Information includes: Table S1, MIC values of Gad-1 with supplemented Zn^{2+}; Figure S1, Mass spectrometry data of Gad-1 with Zn^{2+} and a Zincon titration assay showing low affinity binding; Figure S2, EPR spectrum of H3A in MOPS buffer (pH 7.0) showing shf splitting; Figure S3, ITC binding curve for Gad-1, fit with a multiple binding site model; Table S2, Thermodynamic values from ITC experiments with Gad-1 and Zn^{2+}; Figure S4, Helical wheel diagram of Gad-1

Author Information

Corresponding Author

Alfredo M. Angeles-Boza - Department of Chemistry and Institute of Materials Science, University of Connecticut, Storrs, Connecticut 06269, United States

Present Addresses

Jasmin Portelinha – jasmin.portelinha@uconn.edu, Department of Chemistry, University of Connecticut, Storrs, Connecticut 06269, United States

Kara Heilemann – kara.heilemann@uconn.edu, Department of Chemistry, University of Connecticut, Storrs, Connecticut 06269, United States

Jing Jin - jinjq@bc.edu, Magnetic Resonance Center, Boston College, 2609 Beacon Street, Chestnut Hill, MA 02467

Author Contributions

JP completed all of the experimental work. KH contributed to the β-galactosidase leakage and lipid (per)oxidation experiments. JJ contributed the EPR simulation data collected. JP wrote the manuscript and AMA-B edited the manuscript and advised.

Funding

This material is based upon work supported by the National Science Foundation under Grant [MCB1715494 to AMA-B]. The National Biomedical Center for Advanced Electron Spin Resonance Technology (ACERT) is supported by NIH/NIGMS [P41GM103521].

Notes

The authors declare no competing financial interests.

Acknowledgment

We would like to thank the Graf and Nyholm labs at UConn for the generous donation of *A. hydrophila* and *V. harveyi* respectively. We would also like to thank Dr. Cady at UConn and Dr. Dzikovski at Cornell for sharing their expertise with EPR and Dr. Heidi Erlandsen at UConn for sharing her expertise in ITC. Lastly, JP thanks David Lei, Arthur Parzygnat, and Jessica A. Martin for helpful conversations and meaningful comments.

Abbreviations

AMP, Antimicrobial peptide; amino terminal copper and nickel, ATCUN; isothermal titration calorimetry, ITC; electrospray ionization mass spectrometry, ESI-MS; electron paramagnetic resonance, EPR; minimum inhibitory concentration, MIC; minimum bactericidal concentration, MBC; time kill kinetics, TKK; 3-morpholinopropane-1-sulfonic acid, MOPS; 2-(N-morpholino)ethanesulfonic acid, MES; 2-[4-(2-hydroxyethyl)piperazin-1-yl]ethanesulfonic acid, HEPES; triethylenetetramine, TETA; circular dichroism, CD; SDS; sodium dodecyl sulfate, trifluoroethanol, TFE; 1-palmitoyl-2-oleoyl-sn-glycero-3-phosphatidylglycerol, POPG; 1-palmitoyl-2-oleoyl-sn-glycero-3-phosphocholine, POPC; reactive oxygen species, ROS.

Keywords

Lipid (per)oxidation, Antimicrobial peptide, Reactive oxygen species, Piscidins, Cu^{2+}-mediated activity, Histidine

REFERENCES

(1) Der Torossian Torres, M.; De La Fuente-Nunez, C. Reprogramming Biological Peptides to Combat Infectious Diseases. *Chem. Commun.* **2019**, *55* (100), 15020–15032. https://doi.org/10.1039/c9cc07898c.

(2) Wang, G.; Li, X.; Wang, Z. APD3: The Antimicrobial Peptide Database as a Tool for Research and Education. *Nucleic Acids Res.* **2016**, *44* (D1), D1087–D1093. https://doi.org/10.1093/nar/gkv1278.

(3) Yount, N. Y.; Weaver, D. C.; Lee, E. Y.; Lee, M. W.; Wang, H.; Chan, L. C.; Wong, G. C. L.; Yeaman, M. R. Unifying Structural Signature of Eukaryotic α-Helical Host Defense Peptides. *Proc. Natl. Acad. Sci. U. S. A.* **2019**, *116* (14), 6944–6953. https://doi.org/10.1073/pnas.1819250116.

(4) Lee, I. H.; Zhao, C.; Cho, Y.; Harwig, S. S. L.; Cooper, E. L.; Lehrer, R. I. Clavanins, α-Helical Antimicrobial Peptides from Tunicate Hemocytes. *FEBS Lett.* **1997**, *400* (2), 158–162. https://doi.org/10.1016/S0014-5793(96)01374-9.

(5) Silphaduang, U.; Noga, E. J. Peptide Antibiotics in Mast Cells of Fish. *Nature* **2001**, *414* (6861), 268–269. https://doi.org/10.1038/35104690.

(6) Situ, H.; Bobek, L. A. In Vitro Assessment of Antifungal Therapeutic Potential of Salivary Histatin-5, Two Variants of Histatin-5, and Salivary Mucin (MUC7) Domain 1. *Antimicrob. Agents Chemother.* **2000**, *44* (6), 1485–1493. https://doi.org/10.1128/AAC.44.6.1485-1493.2000.

(7) Mulero, I.; Noga, E. J.; Meseguer, J.; García-Ayala, A.; Mulero, V. The Antimicrobial

Peptides Piscidins Are Stored in the Granules of Professional Phagocytic Granulocytes of Fish and Are Delivered to the Bacteria-Containing Phagosome upon Phagocytosis. *Dev. Comp. Immunol.* **2008**, *32* (12), 1531–1538. https://doi.org/10.1016/j.dci.2008.05.015.

(8) Neupane, K. P.; Aldous, A. R.; Kritzer, J. A. Macrocyclization of the ATCUN Motif Controls Metal Binding and Catalysis. *Inorg. Chem.* **2013**, *52* (5), 2729–2735. https://doi.org/10.1021/ic302820z.

(9) Neupane, K. P.; Aldous, A. R.; Kritzer, J. A. Metal-Binding and Redox Properties of Substituted Linear and Cyclic ATCUN Motifs. *J Inorg Biochem* **2014**, *139*, 65–76. https://doi.org/10.1016/j.jinorgbio.2014.06.004.

(10) Libardo, M. D. J.; Bahar, A. A.; Ma, B.; Fu, R.; McCormick, L. E.; Zhao, J.; McCallum, S. A.; Nussinov, R.; Ren, D.; Angeles-Boza, A. M.; Cotten, M. L. Nuclease Activity Gives an Edge to Host-Defense Peptide Piscidin 3 over Piscidin 1, Rendering It More Effective against Persisters and Biofilms. *FEBS J.* **2017**, *284* (21), 3662–3683. https://doi.org/10.1111/febs.14263.

(11) Jin, Y.; Cowan, J. A. DNA Cleavage by Copper-ATCUN Complexes. Factors Influencing Cleavage Mechanism and Linearization of DsDNA. *J. Am. Chem. Soc.* **2005**, *127* (23), 8408–8415. https://doi.org/10.1021/ja0503985.

(12) Joyner, J.; Reichfield, J.; Cowan, J.; Manuscript, A.; Chelates, C. Factors Influencing the DNA Nuclease Activity of Iron, Cobalt, Nickel, and Copper Chelates. *J. Am. Chem. Soc.* **2011**, *133* (39), 15613–15626. https://doi.org/10.1021/ja2052599.

(13) Alexander, J. L.; Thompson, Z.; Cowan, J. A. Antimicrobial Metallopeptides. *ACS Chem. Biol.* **2018**, *13* (4), 844–853. https://doi.org/10.1021/acschembio.7b00989.

(14) Alexander, J. L.; Yu, Z.; Cowan, J. A. Amino Terminal Copper and Nickel Binding Motif Derivatives of Ovispirin-3 Display Increased Antimicrobial Activity via Lipid

Oxidation. *J. Med. Chem.* **2017**, *60* (24), 10047–10055. https://doi.org/10.1021/acs.jmedchem.7b01117.

(15) Hayden, R. M.; Goldberg, G. K.; Ferguson, B. M.; Schoeneck, M. W.; Libardo, M. D. J.; Mayeux, S. E.; Shrestha, A.; Bogardus, K. A.; Hammer, J.; Pryshchep, S.; Lehman, H. K.; McCormick, M. L.; Blazyk, J.; Angeles-Boza, A. M.; Fu, R.; Cotten, M. L. Complementary Effects of Host Defense Peptides Piscidin 1 and Piscidin 3 on DNA and Lipid Membranes: Biophysical Insights into Contrasting Biological Activities. *J. Phys. Chem. B* **2015**, *119* (49), 15235–15246. https://doi.org/10.1021/acs.jpcb.5b09685.

(16) Campagna, S.; Saint, N.; Molle, G.; Aumelas, A. Structure and Mechanism of Action of the Antimicrobial Peptide Piscidin. *Biochemistry* **2007**, *46* (7), 1771–1778. https://doi.org/10.1021/bi0620297.

(17) Djoko, K. Y.; Ong, C. Y.; Walker, M. J.; McEwan, A. G. The Role of Copper and Zinc Toxicity in Innate Immune Defense against Bacterial Pathogens. *J. Biol. Chem.* **2015**, *290* (31), 18954–18961. https://doi.org/10.1074/jbc.R115.647099.

(18) Wagner, D.; Maser, J.; Lai, B.; Cai, Z.; Barry, C. E.; Höner, K.; David, G.; Bermudez, L. E.; Iii, C. E. B. Elemental Analysis of Mycobacterium Avium-, Mycobacterium Tuberculosis-, and Mycobacterium Smegmatis-Containing Phagosomes Indicates Pathogen-Induced Microenvironments within the Host Cell's Endosomal System. *J. Immunol.* **2005**, *174* (3), 1491–1500. https://doi.org/10.4049/jimmunol.174.3.1491.

(19) White, C.; Lee, J.; Kambe, T.; Fritsche, K.; Petris, M. J. A Role for the ATP7A Copper-Transporting ATPase in Macrophage Bactericidal Activity. *J. Biol. Chem.* **2009**, *284* (49), 33949–33956. https://doi.org/10.1074/jbc.M109.070201.

(20) Botella, H.; Peyron, P.; Levillain, F.; Poincloux, R.; Poquet, Y.; Brandli, I.; Wang, C.; Tailleux, L.; Tilleul, S.; Charrire, G. M.; Waddell, S. J.; Foti, M.; Lugo-Villarino, G.; Gao, Q.; Maridonneau-Parini, I.; Butcher, P. D.; Castagnoli, P. R.; Gicquel, B.; De

Chastellier, C.; Neyrolles, O. Mycobacterial P1-Type ATPases Mediate Resistance to Zinc Poisoning in Human Macrophages. *Cell Host Microbe* **2011**, *10* (3), 248–259. https://doi.org/10.1016/j.chom.2011.08.006.

(21) Zahran, E.; Noga, E. J. Evidence for Synergism of the Antimicrobial Peptide Piscidin 2 with Antiparasitic and Antioomycete Drugs. *J. Fish Dis.* **2010**, *33* (12), 995–1003. https://doi.org/10.1111/j.1365-2761.2010.01205.x.

(22) Ruangsri, J.; Salger, S. A.; Caipang, C. M. A.; Kiron, V.; Fernandes, J. M. O. Differential Expression and Biological Activity of Two Piscidin Paralogues and a Novel Splice Variant in Atlantic Cod (Gadus Morhua L.). *Fish Shellfish Immunol.* **2012**, *32* (3), 396–406. https://doi.org/10.1016/j.fsi.2011.11.022.

(23) McDonald, M.; Mannion, M.; Pike, D.; Lewis, K.; Flynn, A.; Brannan, A. M.; Browne, M. J.; Jackman, D.; Madera, L.; Power Coombs, M. R.; Hoskin, D. W.; Rise, M. L.; Booth, V. Structure-Function Relationships in Histidine-Rich Antimicrobial Peptides from Atlantic Cod. *Biochim. Biophys. Acta - Biomembr.* **2015**, *1848* (7), 1451–1461. https://doi.org/10.1016/j.bbamem.2015.03.030.

(24) Portelinha, J.; Angeles-Boza, A. M. The Antimicrobial Peptide Gad-1 Clears Pseudomonas Aeruginosa Biofilms under Cystic Fibrosis Conditions. *ChemBioChem* **2021**. https://doi.org/10.1002/cbic.202000816.

(25) Juliano, S. A.; Serafim, L. F.; Duay, S. S.; Heredia Chavez, M.; Sharma, G.; Rooney, M.; Comert, F.; Pierce, S.; Radulescu, A.; Cotten, M. L.; Mihailescu, M.; May, E. R.; Greenwood, A. I.; Prabhakar, R.; Angeles-Boza, A. M. A Potent Host Defense Peptide Triggers DNA Damage and Is Active against Multidrug-Resistant Gram-Negative Pathogens. *ACS Infect. Dis.* **2020**, *6* (5), 1250–1263. https://doi.org/10.1021/acsinfecdis.0c00051.

(26) Juliano, S. A.; Pierce, S.; Demayo, J. A.; Balunas, M. J.; Angeles-Boza, A. M.

Exploration of the Innate Immune System of Styela Clava: Zn2+ Binding Enhances the Antimicrobial Activity of the Tunicate Peptide Clavanin A. *Biochemistry* **2017**, *56* (10), 1403–1414. https://doi.org/10.1021/acs.biochem.6b01046.

(27) Libardo, M. D.; Cervantes, J. L.; Salazar, J. C.; Angeles-Boza, A. M. Improved Bioactivity of Antimicrobial Peptides by Addition of Amino-Terminal Copper and Nickel (ATCUN) Binding Motifs. *ChemMedChem* **2014**, *9* (8), 1892–1901. https://doi.org/10.1002/cmdc.201402033.

(28) Quinn, C. F.; Carpenter, M. C.; Croteau, M. L.; Wilcox, D. E. *Isothermal Titration Calorimetry Measurements of Metal Ions Binding to Proteins*, 1st ed.; Elsevier Inc., 2016; Vol. 567. https://doi.org/10.1016/bs.mie.2015.08.021.

(29) Micsonai, A.; Wien, F.; Bulyáki, É.; Kun, J.; Moussong, É.; Lee, Y. H.; Goto, Y.; Réfrégiers, M.; Kardos, J. BeStSel: A Web Server for Accurate Protein Secondary Structure Prediction and Fold Recognition from the Circular Dichroism Spectra. *Nucleic Acids Res.* **2018**, *46* (W1), W315–W322. https://doi.org/10.1093/nar/gky497.

(30) Harford, C.; Sarkar, B. Amino Terminal Cu(II)- and Ni(II)-Binding (ATCUN) Motif of Proteins and Peptides: Metal Binding, DNA Cleavage, and Other Properties. *Acc. Chem. Res.* **1997**, *30* (3), 123–130. https://doi.org/10.1021/ar9501535.

(31) Lawson, M. K.; Valko, M.; Cronin, M. T. D.; Jomová, K. Chelators in Iron and Copper Toxicity. *Curr. Pharmacol. Reports* **2016**, *2* (6), 271–280. https://doi.org/10.1007/s40495-016-0068-8.

(32) Fernández-Mazarrasa, C.; Mazarrasa, O.; Calvo, J.; Del Arco, A.; Martínez-Martínez, L. High Concentrations of Manganese in Mueller-Hinton Agar Increase MICs of Tigecycline Determined by Etest. *J. Clin. Microbiol.* **2009**, *47* (3), 827–829. https://doi.org/10.1128/JCM.02464-08.

(33) Duay, S. S.; Sharma, G.; Prabhakar, R.; Angeles-Boza, A. M.; May, E. R. Molecular

Dynamics Investigation into the Effect of Zinc(II) on the Structure and Membrane Interactions of the Antimicrobial Peptide Clavanin A. *J Phys Chem B* **2019**, *123* (15), 3163–3176. https://doi.org/10.1021/acs.jpcb.8b11496.

(34) Dashper, S. G.; O'Brien-Simpson, N. M.; Cross, K. J.; Paolini, R. A.; Hoffmann, B.; Catmull, D. V.; Malkoski, M.; Reynolds, E. C. Divalent Metal Cations Increase the Activity of the Antimicrobial Peptide Kappacin. *Antimicrob. Agents Chemother.* **2005**, *49* (6), 2322–2328. https://doi.org/10.1128/AAC.49.6.2322-2328.2005.

(35) Lemaitre, B.; Reichhart, J. M.; Hoffmann, J. A. Drosophila Host Defense: Differential Induction of Antimicrobial Peptide Genes after Infection by Various Classes of Microorganisms. *Proc. Natl. Acad. Sci. U. S. A.* **1997**, *94* (26), 14614–14619. https://doi.org/10.1073/pnas.94.26.14614.

(36) Hanson, M. A.; Dostálová, A.; Ceroni, C.; Poidevin, M.; Kondo, S.; Lemaitre, B. Synergy and Remarkable Specificity of Antimicrobial Peptides in Vivo Using a Systematic Knockout Approach. *Elife* **2019**, *8* (e44341), 1–24. https://doi.org/10.7554/elife.44341.

(37) Karlin, K. D.; Zubieta, J. *Copper Coordination Chemistry: Biochemical and Inorganic Perspectives*; 1982.

(38) Antholine, W. E. Chapter 14: Low Frequency EPR of in Proteins. In *Multifrequency ESR of Copper Biophysical Applications*; 1990; pp 417–454.

(39) Pradines, V.; Stroia, A. J.; Faller, P. Amyloid Fibrils: Modulation of Formation and Structure by Copper(II). *New J. Chem.* **2008**, *32* (7), 1189–1194. https://doi.org/10.1039/b719556g.

(40) Gonzalez, P.; Vileno, B.; Bossak, K.; El Khoury, Y.; Hellwig, P.; Bal, W.; Hureau, C.; Faller, P. Cu(II) Binding to the Peptide Ala-His-His, a Chimera of the Canonical Cu(II)-Binding Motifs Xxx-His and Xxx-Zzz-His. *Inorg. Chem.* **2017**, *56* (24), 14870–14879.

https://doi.org/10.1021/acs.inorgchem.7b01996.

(41) Sciortino, G.; Lubinu, G.; Maréchal, J.-D.; Garribba, E. DFT Protocol for EPR Prediction of Paramagnetic Cu(II) Complexes and Application to Protein Binding Sites. *Magnetochemistry* **2018**, *4* (4), 55. https://doi.org/10.3390/magnetochemistry4040055.

(42) Gonzalez, P.; Bossak, K.; Stefaniak, E.; Hureau, C.; Raibaut, L.; Bal, W.; Faller, P. N-Terminal Cu-Binding Motifs (Xxx-Zzz-His, Xxx-His) and Their Derivatives: Chemistry, Biology and Medicinal Applications. *Chem. - A Eur. J.* **2018**, *24* (32), 8029–8041. https://doi.org/10.1002/chem.201705398.

(43) Bhattacharyya, S.; Kumar, S. B.; Dutta, S. K.; Tiekink, E. R. T.; Chaudhury, M. Zinc(II) and Copper(II) Complexes of Pentacoordinating (N4S) Ligands with Flexible Pyrazolyl Arms: Syntheses, Structure, and Redox and Spectroscopic Properties. *Inorg. Chem.* **1996**, *35* (7), 1967–1973. https://doi.org/10.1021/ic950594k.

(44) Hasenknopf, B.; Lehn, J. M.; Baum, G.; Fenske, D. Self-Assembly of a Heteroduplex Helicate from Two Different Ligand Strands and Cu(II) Cations. *Proc. Natl. Acad. Sci. U. S. A.* **1996**, *93* (4), 1397–1400. https://doi.org/10.1073/pnas.93.4.1397.

(45) Rai, R. K.; De Angelis, A.; Greenwood, A. I.; Opella, S. J.; Cotten, M. Metal-Ion Binding to Host Defense Peptide Piscidin 3 Observed in Phospholipid Bilayers by Magic Angle Spinning Solid-State NMR. *ChemPhysChem* **2019**, *20* (2), 295–301. https://doi.org/10.1002/cphc.201800855.

(46) Yorita, H.; Otomo, K.; Hiramatsu, H.; Toyama, A.; Miura, T.; Takeuchi, H. Evidence for the Cation-π Interaction between Cu2+ and Tryptophan. *J. Am. Chem. Soc.* **2008**, *130* (46), 15266–15267. https://doi.org/10.1021/ja807010f.

(47) Zoroddu, M. A.; Medici, S.; Peana, M. Copper and Nickel Binding in Multi-Histidinic Peptide Fragments. *J. Inorg. Biochem.* **2009**, *103* (9), 1214–1220. https://doi.org/10.1016/j.jinorgbio.2009.06.008.

(48) Seebauer, E. G.; Duliba, E. P.; Scogin, D. A.; Gennis, R. B.; Belford, R. L. EPR Evidence on the Structure of the Copper(II)-Bacitracin A Complex. *J. Am. Chem. Soc.* **1983**, *105* (15), 4926–4929. https://doi.org/10.1021/ja00353a015.

(49) Peisach, J.; Blumberg, W. E. Structural Implications Derived from the Analysis of Electron Paramagnetic Resonance Spectra of Natural and Artificial Copper Proteins. *Arch. Biochem. Biophys.* **1974**. https://doi.org/10.1016/0003-9861(74)90298-7.

(50) Zhang, X.; Liu, X.; Phillips, D. L.; Zhao, C. Hydrolysis Mechanisms of BNPP Mediated by Facial Copper(II) Complexes Bearing Single Alkyl Guanidine Pendants: Cooperation between the Metal Centers and the Guanidine Pendants. *Dalt. Trans.* **2016**, *45* (4), 1593–1603. https://doi.org/10.1039/c5dt03949e.

(51) Wu, Z.; Fernandez-Lima, F. A.; Russell, D. H. Amino Acid Influence on Copper Binding to Peptides: Cysteine versus Arginine. *J. Am. Soc. Mass Spectrom.* **2010**, *21* (4), 522–533. https://doi.org/10.1016/j.jasms.2009.12.020.

(52) Piscopo, M.; Trifuoggi, M.; Scarano, C.; Gori, C.; Giarra, A.; Febbraio, F. Relevance of Arginine Residues in Cu(II)-Induced DNA Breakage and Proteinase K Resistance of H1 Histones. *Sci. Rep.* **2018**, *8* (1), 1–10. https://doi.org/10.1038/s41598-018-25784-z.

(53) Miyamoto, T.; Kamino, S.; Odani, A.; Hiromura, M.; Enomoto, S. Basicity of N-Terminal Amine in ATCUN Peptide Regulates Stability Constant of Albumin-like Cu2+ Complex. *Chem. Lett.* **2013**, *42* (9), 1099–1101. https://doi.org/10.1246/cl.130405.

(54) Mlynarz, P.; Gaggelli, N.; Panek, J.; Stasiak, M.; Valensin, G.; Kowalik-Jankowska, T.; Leplawy, M. L.; Latajka, Z.; Koziowski, H. How the α-Hydroxymethylserine Residue Stabilizes Oligopeptide Complexes with Nickel(II) and Copper(II) Ions. *J. Chem. Soc., Dalt. Trans.* **2000**, No. 7, 1033–1038. https://doi.org/10.1039/a909354k.

(55) Bal, W.; Chmurny, G. N.; Hilton, B. D.; Sadler, P. J.; Tucker, A. Axial Hydrophobic Fence in Highly-Stable Ni(II) Complex of Des-Angiotensinogen N-Terminal Peptide. *J.*

Am. Chem. Soc. **1996**, *118* (19), 4727–4728. https://doi.org/10.1021/ja953988j.

(56) Demarse, N. A.; Quinn, C. F.; Eggett, D. L.; Russell, D. J.; Hansen, L. D. Calibration of Nanowatt Isothermal Titration Calorimeters with Overflow Reaction Vessels. *Anal. Biochem.* **2011**, *417* (2), 247–255. https://doi.org/10.1016/j.ab.2011.06.014.

(57) Zhang, Y.; Akilesh, S.; Wilcox, D. E. Isothermal Titration Calorimetry Measurements of Ni(II) and Cu(II) Binding to His, GlyGlyHis, HisGlyHis, and Bovine Serum Albumin: A Critical Evaluation. *Inorg. Chem.* **2000**, *39* (14), 3057–3064. https://doi.org/10.1021/ic000036s.

(58) Płonka, D.; Bal, W. The N-Terminus of Hepcidin Is a Strong and Potentially Biologically Relevant Cu(II) Chelator. *Inorganica Chim. Acta* **2018**, *472*, 76–81. https://doi.org/10.1016/j.ica.2017.06.051.

(59) Rózga, M.; Sokołowska, M.; Protas, A. M.; Bal, W. Human Serum Albumin Coordinates Cu(II) at Its N-Terminal Binding Site with 1 PM Affinity. *J. Biol. Inorg. Chem.* **2007**, *12* (6), 913–918. https://doi.org/10.1007/s00775-007-0244-8.

(60) Irving, B. H.; Williams, R. J. P. The Stability of Transition-Metal Complexes. *J. Chem. Soc.* **1953**, 3192–3210. https://doi.org/10.1039/JR9530003192.

(61) Sørensen, K. K.; Sveinbjørnsson, B.; Dalmo, R. A.; Smedsrød, B.; Bertheussen, K. Isolation, Cultivation and Characterization of Head Kidney Macrophages from Atlantic Cod, Gadus Morhua L. *J. Fish Dis.* **1997**, *20* (2), 93–107. https://doi.org/10.1046/j.1365-2761.1997.d01-112.x.

(62) Ruangsri, J.; Fernandes, J. M. O.; Rombout, J. H. W. M.; Brinchmann, M. F.; Kiron, V. Ubiquitous Presence of Piscidin-1 in Atlantic Cod as Evidenced by Immunolocalisation. *BMC Vet. Res.* **2012**, *8* (46), 1–13. https://doi.org/10.1186/1746-6148-8-46.

(63) Lee, S. A.; Kim, Y. K.; Lim, S. S.; Zhu, W. L.; Ko, H.; Shin, S. Y.; Hahm, K. S.; Kim, Y. Solution Structure and Cell Selectivity of Piscidin 1 and Its Analogues. *Biochemistry*

2007, *46* (12), 3653–3663. https://doi.org/10.1021/bi062233u.

(64) Overton, K.; Greer, H. M.; Ferguson, M. A.; Spain, E. M.; Elmore, D. E.; Núñez, M. E.; Volle, C. B. Qualitative and Quantitative Changes to Escherichia Coli during Treatment with Magainin 2 Observed in Native Conditions by Atomic Force Microscopy. *Langmuir* **2020**, *36* (2), 650–659. https://doi.org/10.1021/acs.langmuir.9b02726.

(65) Wade, H. M.; Darling, L. E. O.; Elmore, D. E. Hybrids Made from Antimicrobial Peptides with Different Mechanisms of Action Show Enhanced Membrane Permeabilization. *Biochim. Biophys. Acta - Biomembr.* **2019**, *1861* (10), 182980. https://doi.org/10.1016/j.bbamem.2019.05.002.

(66) Libardo, M. D. J.; Gorbatyuk, V. Y.; Angeles-Boza, A. M. Central Role of the Copper-Binding Motif in the Complex Mechanism of Action of Ixosin: Enhancing Oxidative Damage and Promoting Synergy with Ixosin B. *ACS Infect. Dis.* **2016**, *2* (1), 71–81. https://doi.org/10.1021/acsinfecdis.5b00140.

(67) Wang, T.-Y.; Libardo, M. D. J.; Angeles-Boza, A. M.; Pellois, J.-P. Membrane Oxidation in Cell Delivery and Cell Killing Applications. *ACS Chem. Biol.* **2017**, *12* (5), 1170–1182. https://doi.org/10.1021/acschembio.7b00237.

(68) Dwyer, D. J.; Belenky, P. A.; Yang, J. H.; Cody MacDonald, I.; Martell, J. D.; Takahashi, N.; Chan, C. T. Y.; Lobritz, M. A.; Braff, D.; Schwarz, E. G.; Ye, J. D.; Pati, M.; Vercruysse, M.; Ralifo, P. S.; Allison, K. R.; Khalil, A. S.; Ting, A. Y.; Walker, G. C.; Collins, J. J. Antibiotics Induce Redox-Related Physiological Alterations as Part of Their Lethality. *Proc. Natl. Acad. Sci. U. S. A.* **2014**, *111* (20), E2100–E2109. https://doi.org/10.1073/pnas.1401876111.

(69) Choi, H.; Yang, Z.; Weisshaar, J. C. Single-Cell, Real-Time Detection of Oxidative Stress Induced in Escherichia Coli by the Antimicrobial Peptide CM15. *Proc. Natl. Acad. Sci. U. S. A.* **2015**, *112* (3), E303–E310.

https://doi.org/10.1073/pnas.1417703112.

(70) Belenky, P.; Ye, J. D.; Porter, C. B. M.; Cohen, N. R.; Lobritz, M. A.; Ferrante, T.; Jain, S.; Korry, B. J.; Schwarz, E. G.; Walker, G. C.; Collins, J. J. Bactericidal Antibiotics Induce Toxic Metabolic Perturbations That Lead to Cellular Damage. *Cell Rep.* **2015**, *13* (5), 968–980. https://doi.org/10.1016/j.celrep.2015.09.059.

(71) Van Acker, H.; Gielis, J.; Acke, M.; Cools, F.; Cos, P.; Coenye, T. The Role of Reactive Oxygen Species in Antibiotic-Induced Cell Death in Burkholderia Cepacia Complex Bacteria. *PLoS One* **2016**, *11* (7), 1–20. https://doi.org/10.1371/journal.pone.0159837.

(72) Hussain, A.; AlAjmi, M. F.; Rehman, M. T.; Amir, S.; Husain, F. M.; Alsalme, A.; Siddiqui, M. A.; AlKhedhairy, A. A.; Khan, R. A. Copper (II) Complexes as Potential Anticancer and Nonsteroidal Anti-Inflammatory Agents: In Vitro and in Vivo Studies. *Sci. Rep.* **2019**, *9* (1), 1–17. https://doi.org/10.1038/s41598-019-41063-x.

(73) Santini, C.; Pellei, M.; Gandin, V.; Porchia, M.; Tisato, F.; Marzano, C. Advances in Copper Complexes as Anticancer Agents. *Chem. Rev.* **2014**, *114* (1), 815–862. https://doi.org/10.1021/cr400135x.

(74) Ng, C. H.; Kong, S. M.; Tiong, Y. L.; Maah, M. J.; Sukram, N.; Ahmad, M.; Khoo, A. S. B. Selective Anticancer Copper(II)-Mixed Ligand Complexes: Targeting of ROS and Proteasomes. *Metallomics* **2014**, *6* (4), 892–906. https://doi.org/10.1039/c3mt00276d.

(75) Khatami, M. H.; Bromberek, M.; Saika-Voivod, I.; Booth, V. Molecular Dynamics Simulations of Histidine-Containing Cod Antimicrobial Peptide Paralogs in Self-Assembled Bilayers. *Biochim. Biophys. Acta - Biomembr.* **2014**, *1838* (11), 2778–2787. https://doi.org/10.1016/j.bbamem.2014.07.013.

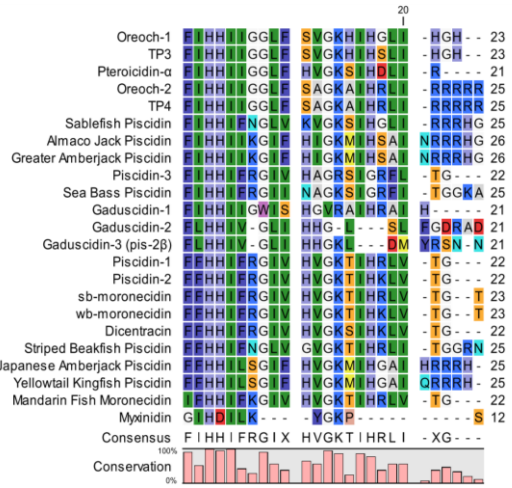

Figure 1. Alignment showing piscidin peptide with ATCUN motifs. Conservation of His residues in positions 3, 4, 11, and 17 is shown here. UniProt accession numbers are as follows if available: **Piscidin-1** Q8UUG0, **Piscidin-2** Q8UUG2, **Piscidin 3** P0C006, **TP3** L0CMD2, **TP4** L0CKG3, **Gaduscidin-1** D4HRB8, **Gaduscidin-2** E2EZU3, **pis2β** E7D8W6, **Dicentracin** P59906, **Mandarin Fish Moronecidin** Q2VWH5, **Yellowtail Kingfish Piscidin** A0A1W6FCA1, **Almaco Jack Piscidin** A0A2P1CNR7, **Sablefish Piscidin** C3KHI8, **Striped Beakfish Piscidin** M4ZUG8, and **Greater Amberjack Piscidin** A0A3G2LYX4.

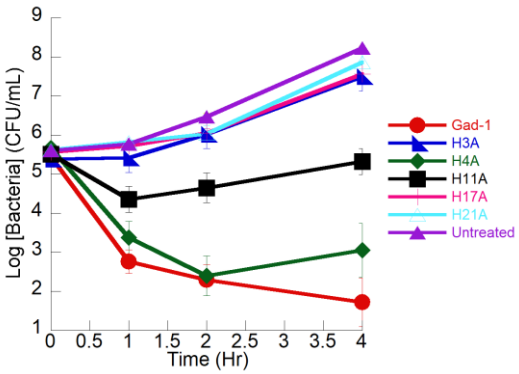

Figure 2. TKK data showing that Gad-1, H4A, and H11A are bactericidal at 4 μM, while the other mutants are associated with Cu^{2+} binding residues are bacteriostatic at 4 μM against *E. coli* in MHB (pH ~7.0).

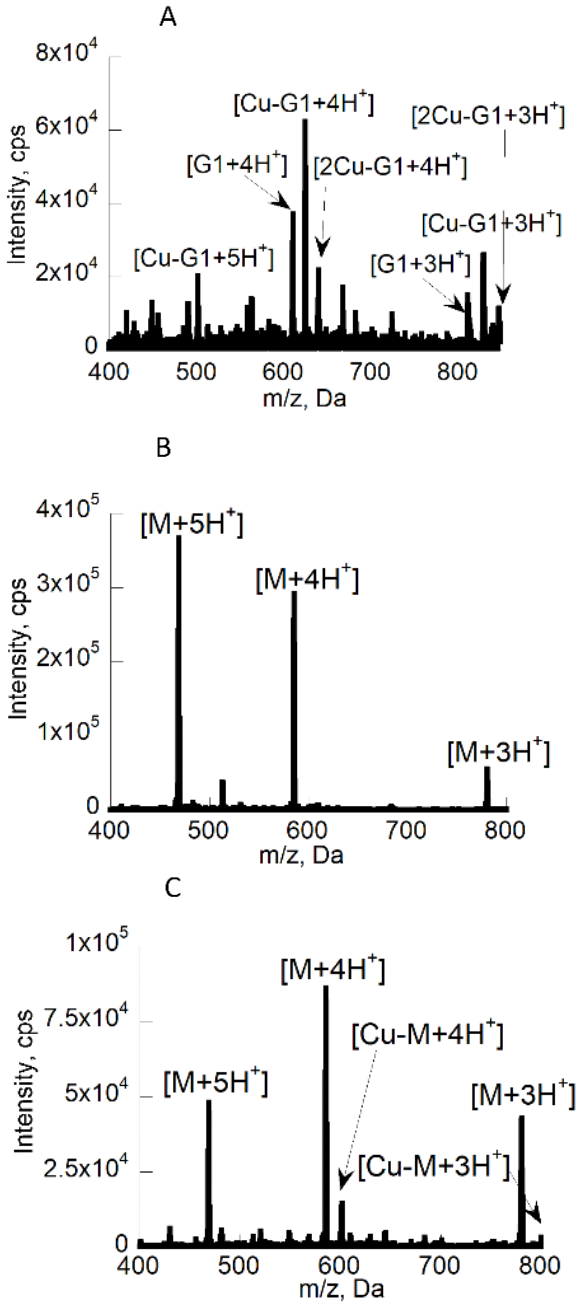

Figure 3. ESI-MS data for peptide in the presence of five times Cu^{2+}. (A) Mass spectrum for Gad-1 with peaks that corresponded to 1:1 and 1:2 Gad-1:Cu^{2+} stoichiometry confirming that Gad-1 can bind to up to two Cu^{2+} ions. (B) The necessity for His3 and His17 for Cu^{2+} binding was revealed in the spectrum for the H3,17A mutant, where no peaks were associated with bound peptide. (C) The spectrum of H3A-H11A shows 1:1 binding of the Cu^{2+} at the HXXXH site that does not involve His11, in addition to apo-peptide.

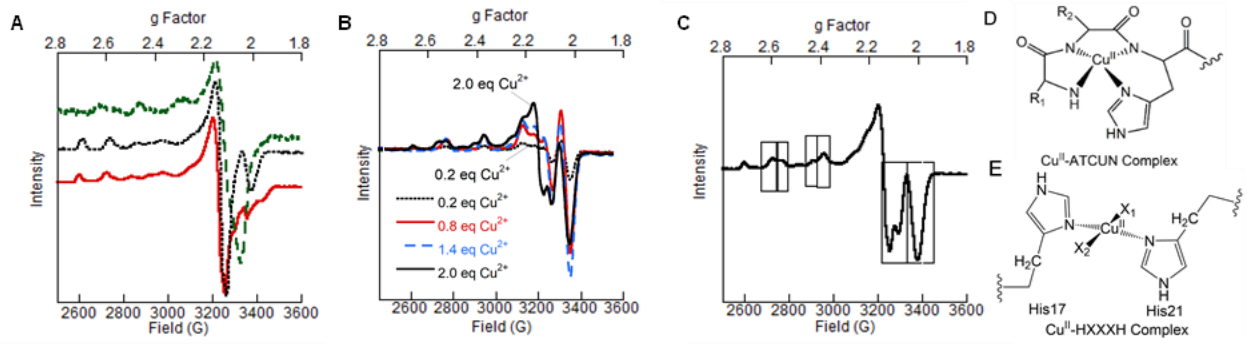

Figure 4. EPR spectra recorded at 50 K in 10% glycerol using microwave frequency of 9.32 GHz, microwave power was 0.06325 mW, and power attenuation of 35 dB. (A) EPR spectra in MOPS buffer at pH 7.0 with 0.9 equivalents Cu^{2+} comparing H3A (dashed line), Gad-1 (dotted line), and H17A-H21A (solid line), where Gad-1 appears to display multiple species. (B) Gad-1 titration in MOPS buffer at pH 7.0 with up to 2.0 equivalents of Cu^{2+}, showing the addition of peaks corresponding to the ATCUN and HXXXH sites. (C) EPR spectra of Gad-1 in 50% TFE:MOPS buffer with 0.9 equivalents Cu^{2+} exhibits multiple species (boxed) when the peptide is in a helical conformation that correspond to the ATCUN and HXXXH sites. (D) Cu^{2+}-ATCUN complex. (E) Cu^{2+}-HXXXH complex, where X_1 is nitrogen and X_2 is either water or nitrogen.

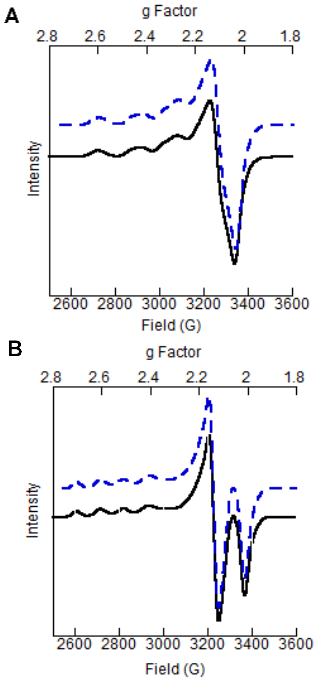

Figure 5. Simulation data (dashed line) for EPR compared to experimental data 1 in MOPS buffer (solid line). (A) H3A was confirmed to form one species with 0.9 equivalents of Cu^{2+}, likely the HXXXH site bound to Cu^{2+}. (B) H17A-H21A with one major and one minor species in the presence of 2 equivalents of Cu^{2+}.

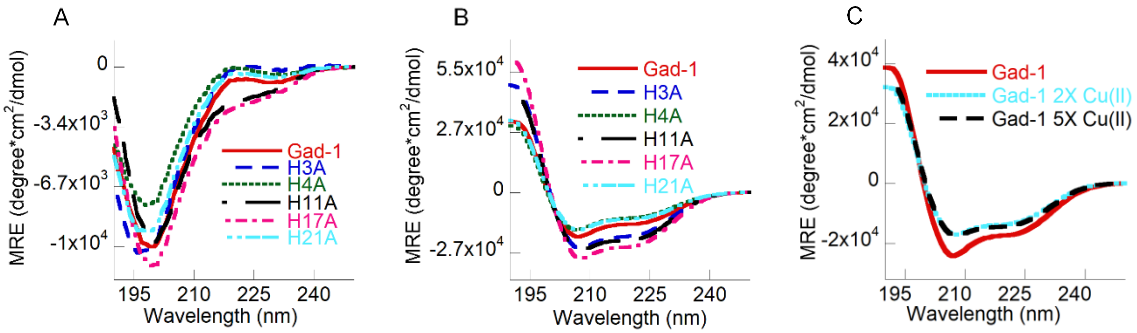

Figure 6. CD data represented by mean residue ellipticity (MRE). (A) 50 μM of disordered peptides in H_2O (B) α-helical peptides in 50% TFE and H_2O (C) Gad-1 in an α-helical conformation with (two times dotted line, five times dashed line) and without (solid line) added Cu^{2+} showing no major change in helicity that could affect the antimicrobial activity.

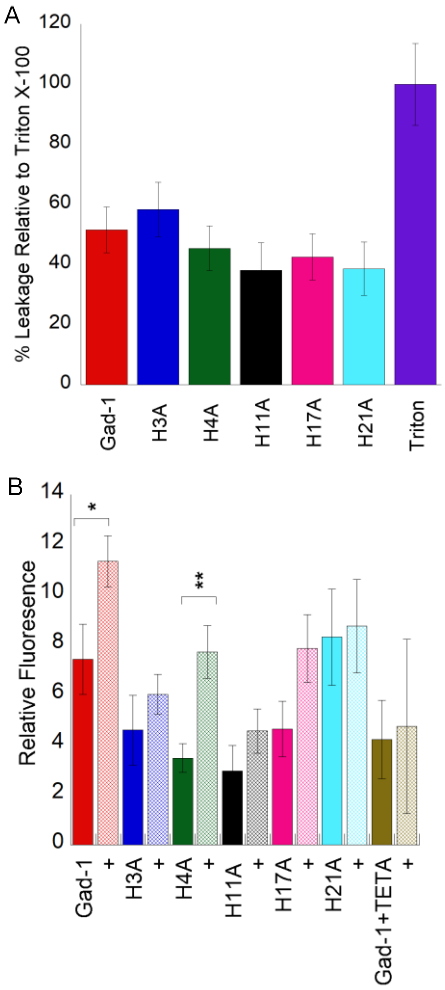

Figure 7. (A) β-galactosidase data indicating percent leakage of cellular contents in the presence of 2 μM peptide relative to 0.1% Triton X-100 in pH 7.4 PBS, where the absorbance of cells alone was subtracted out. (B) Lipid (per)oxidation as assessed by a standard TBARS assay using 20 mM HEPES and 100 mM NaCl buffer at pH 7.4, where "+" denotes that 2 μM Cu^{2+} was added to 4 μM peptide. The fluorescence of the cells alone was subtracted from other values before plotting. Gad-1 and H4A both significantly (where * is $p<0.05$ and ** is $p<0.01$) increase lipid (per)oxidation levels in the presence of Cu^{2+}, while H3A, H11A, H17A, and H21A showed no change in amount of lipid (per)oxidation with Cu^{2+}. This data highlights the importance of Cu^{2+} binding on the multi-hit mechanism of action for Gad-1

Tables

Table 1. Summary of MIC and MBC values (μM) for Gad-1 and mutants in MHB (pH ~7.0), where * indicates that the metal chelator TETA was added.

	MIC				**MBC**			
Peptide	***E. coli***	****E. coli***	***V. harveyi***	***A. hydrophila***	***E. coli***	****E. coli***	***V. harveyi***	***A. hydrophila***
Gad-1	2	16	8	16	2	16	16	16
H3A	16	16	32	>128	16	32	32	--
H4A	2	16	32	16	2	32	32	16
H11A	8	16	64	>128	8	16	64	--
H17A	8	16	16	>128	8	32	32	--
H21A	4	16	16	16	4	16	32	16

Table 2. EPR data for peptide-Cu^{2+} complexes (1:0.9 peptide:Cu^{2+}) represented by calculated g factor and hyperfine splitting (A), where $g_{\parallel}/A_{\parallel}$ and $g_{\perp}/A_{\perp}$ for Gad-1 is g_z/A_z and g_y/A_y due to the rhombic spectrum

Peptide	$g_{\perp}$	$A_{\perp} \times 10^{-4}$ (cm^{-1})	g_x	$A_x \times 10^{-4}$ (cm^{-1})	$g_{\parallel}$	$A_{\parallel} \times 10^{-4}$ (cm^{-1})	$g_{\parallel}/A_{\parallel}$
Gad-1:Cu^{2+}	2.079	121	2.008	100.8	2.266	158.99	142.53
H3A:Cu^{2+}	2.052	166.5	--	--	2.265	175.08	129.35
H17A-H21A:Cu^{2+}	2.079	116	--	--	2.268	160.16	141.62

Table 3. Best fit parameters of ITC data for Cu^{2+} binding with corrected values for MOPS buffer (pH 7.0) for Gad-1 and the H4A mutant, where both can coordinate two Cu^{2+} ions.

	MOPS Buffer pH 7.0				MES Buffer pH 5.5			
	Gad-1		H4A		Gad-1		H4A	
	ATCUN	HXXXH	ATCUN	HXXXH	ATCUN	HXXXH	ATCUN	HXXXH
K_d (M)	5.46×10^{-13}	5.92×10^{-10}	2.19×10^{-13}	3.99×10^{-9}	9.32×10^{-7}	1.07×10^{-4}	1.70×10^{-7}	1.37×10^{-4}
n	1.62	1.31	1.21	1.15	0.70	0.80	0.99	0.68
ΔH (kJ/mol)	-0.95	-25.23	-1.70	0.39	11.4	-15.86	10.38	-0.086
ΔS (J/molK)	120.25	27.17	112.55	46.50	153.7	22.84	164.5	78.19
ΔG (kJ/mol)	-36.80	-33.33	-35.23	-14.25	-34.43	-22.67	-38.64	-23.39

Table 4. Best fit parameters of ITC data for Cu^{2+} binding with corrected values for MOPS buffer (pH 7.0) for the H17A-H21A double mutant and H3A mutant.

	MOPS Buffer pH 7.0			MES Buffer pH 5.5	
	H17,21A ATCUN	**H17,21A HXXXH**	**H3A**	**H17,21A**	**H3A**
K_d (M)	1.18×10^{-13}	2.88×10^{-8}	4.22×10^{-10}	8.26×10^{-7}	2.00×10^{-4}
n	1.03	1.20	1.39	0.93	1.05
ΔH (kJ/mol)	-4.11	-40.37	-2.46	4.73	-15.12
ΔS (J/molK)	121.05	11.73	46.62	132.45	20.14
ΔG (kJ/mol)	-40.18	-43.87	-16.36	-34.74	-21.21

Table 5. Summary of percent helicity and percent β-sheet in 50:50 TFE:H_2O and percent leakage of β-galactosidase as compared to Triton X-100

Peptide	Percent β-sheet	Percent Helicity	Percent Leakage
Gad-1	7.1	43.8	51.64
H3A	5.8	56.6	58.36
H4A	18.4	33.2	45.44
H11A	4.8	56.4	38.15
H17A	0	50.9	42.59
H21A	20.1	34.3	38.64
1:2 Gad-1:Cu^{2+}	8.9	43.7	--
1:5 Gad-1:Cu^{2+}	7.6	43.9	--

Graphical Abstract

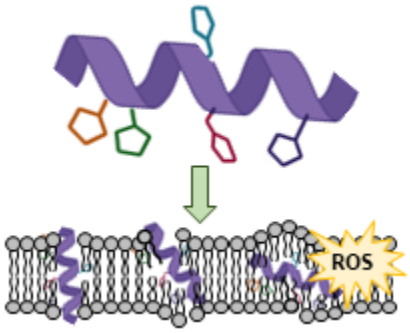

Gaduscidin-1 (Gad-1) is a His-rich antimicrobial peptide that can bind to two Cu^{2+} ions with high affinity at neutral and low pH. Cu^{2+} potentiates the antimicrobial activity against *Escherichia coli* and activates the ability for Gad-1 to (per)oxidize lipids, as well as form pores in bacterial membranes.